Real-Space Local Dynamics of Molten Inorganic Salts using Van Hove Correlation Function

Yuya Shinohara,[1] Alexander S. Ivanov,[2*] Dmitry Maltsev,[2] Garrett E. Granroth,[3] Douglas L. Abernathy,[3] Sheng Dai,[2,4] Takeshi Egami[1,5]*

[1]Materials Science and Technology Division, Oak Ridge National Laboratory, Oak Ridge, Tennessee 37831, United States. [2]Chemical Sciences Division, Oak Ridge National Laboratory, Oak Ridge, Tennessee 37831, United States. [3]Neutron Scattering Division, Oak Ridge National Laboratory, Oak Ridge, Tennessee 37831, United States. [4]Department of Chemistry, University of Tennessee, Knoxville, Tennessee 37996, United States. [5]Department of Materials Science and Engineering and Department of Physics and Astronomy, University of Tennessee, Knoxville, Tennessee 37996, United States.

AUTHOR INFORMATION

Corresponding Author

*Yuya Shinohara: shinoharay@ornl.gov

*Alexander S. Ivanov: ivanova@ornl.gov

Abstract

Molten inorganic salts attract resurgent attention because of their unique physicochemical properties, making them promising media for next generation concentrating solar power systems and molten salt reactors. The dynamics of these highly disordered ionic media is largely studied by theoretical simulations, while the robust experimental techniques capable of observing local dynamics are not well developed. To provide fundamental insights into the atomic-scale transport properties of molten salts, we report the real-space dynamics of molten magnesium chloride at high temperatures employing the Van Hove correlation function obtained by inelastic neutron scattering. Our results directly depict the distance-dependent dynamics of a molten salt on the picosecond time scale. This study demonstrates the capability of the developed approach to describe the locally correlated- and self-dynamics in molten salts, significantly improving our understanding of the interplay between microscopic structural parameters and their dynamics that ultimately control physical properties of condensed matter in extreme environments.

TOC GRAPHICS

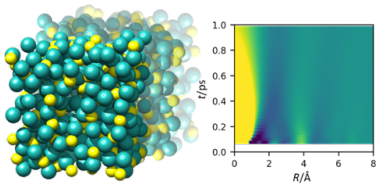

KEYWORDS. Molten salt, liquid dynamics, Van Hove correlation function, inelastic neutron scattering.

Molten inorganic salts have recently garnered tremendous interest from basic science viewpoints due to their unusual physicochemical properties and their applications to high-temperature concentrating solar power receivers and advanced nuclear reactors using molten chloride or fluoride salts.[1–7] In particular, magnesium chloride ($MgCl_2$) is considered to be a typical component of high-temperature heat-transfer fluids and thermal energy storage media in these systems. Although early works on $MgCl_2$ yielded some clues to its structural and dynamic properties,[8–10] the atomic-level dynamics in molten salts remain poorly understood, mainly due to the lack of experimental tools to explore the local dynamics in extreme and harsh environments of molten ionic media. Identifying the putative dynamic mechanisms that ultimately control macroscopic properties of molten salts at the atomic scale could be instrumental to our perception of condensed matter under highly ionic and high temperature conditions.

Recent *ab initio* molecular dynamics (AIMD) simulations coupled with different rate theory models identified the solvation shell dynamics of anions around cations in simple alkali-chloride molten salts.[11,12] These theoretical results show that ion-pair dissociation processes occur on the picoseconds time scale in these systems. To gain more fundamental insights into dynamical behavior of the melts, a reliable experimental technique to capture real-space local dynamics at these short timeframes is needed. However, the conventional pair distribution function (PDF) approach based on total neutron/X-ray scattering yields only a snap-shot or static description of liquids. Alternatively, quasielastic and inelastic scattering of neutron/X-rays can be used to obtain the dynamic structure factor $S(Q,E)$ and the intermediate scattering function, $F(Q,t)$, of molten salt[13], where Q and E are the momentum and energy transfer, respectively. These quantities provide information about the molecular dynamics in liquids in reciprocal space. Usually, the Q-range is limited to a low-Q regime which corresponds to the reciprocal of multiple jumps of molecules/ions.

The low-Q information is useful when discussing a long-range diffusive behavior but is not suitable for describing the local dynamics. There is a dearth of experimental tools to study the molecular-level local dynamics in molten salts.

To identify the atomic-level motion in liquids, an approach using the Van Hove correlation function (VHF)—a pair correlation function in real-space and time—has been developed.[14–18] The VHF is given by

$$G(R,t) = \frac{1}{4\pi\rho N R^2}\sum_{i,j}\delta\big(R - \left|\boldsymbol{r}_i(0) - \boldsymbol{r}_j(t)\right|\big),$$

where ρ is the average number density of particles, N is the number of particles in the system, $\boldsymbol{r}_i(t)$ is the position of the ith particle at time t, and $\delta(r)$ is Dirac's delta function.[19] $G(R,t)$ is composed of a self-part $G_\mathrm{s}(R,t)$ and a distinct part $G_\mathrm{d}(R,t)$. The self-part represents the probability of finding an atom at distance R at time t given that it was at $R = 0$ at $t = 0$. Meanwhile, the distinct part represents the probability of finding an atom at distance R at time t given that another particle was at $R = 0$ at $t = 0$. At $t = 0$, $G_\mathrm{d}(R,0)$ is identical with the PDF while $G_\mathrm{s}(R,0)$ is identical to $\delta(r)$ and is usually ignored in PDF analyses. $G(R,t)$ is related to $S(Q,E)$ and $F(Q,t)$ via the Fourier transform; thus, the quasi-elastic and inelastic scattering of neutrons and X-rays can provide $G(R,t)$ experimentally, if the Fourier transform can reliably be carried out.[14,20,21] The main difficulty in this approach is termination errors associated with the Fourier transformation. This issue can be mitigated by measuring the spectra over wide ranges of energy transfer E and momentum transfer Q[14,16]. Recent progress in time-of-flight inelastic neutron scattering[22] as well as high-resolution inelastic X-ray scattering[23,24] reduces the termination errors significantly, and enables us to convert the spectra in reciprocal space into the real-space correlation functions, as demonstrated for water and metallic liquid systems.[14,16,17]

To understand the short-time local dynamics of ions in molten salts, we carried out inelastic neutron scattering (INS) measurements of molten $MgCl_2$ salt at ARCS[25], SNS[26] (see *Methods* for the detail). We first merged the INS spectra taken with different incident neutron energies (20, 40, and 80 meV) such that the spectra with the lower energy are used as much as possible. This approach provides a balance between energy resolution and Q coverage. Figure 1 (top) shows the merged INS spectra of $MgCl_2$ molten salt sealed in quartz capillaries and those of empty quartz capillaries at 875 ˚C, which are cut at $Q = 3.88 \pm 0.05$ and 5.18 ± 0.05 Å^{-1}. A strong elastic signal originates mostly from a vanadium foil that was used to cover the quartz capillaries to avoid damages to the furnace in the unlikely event of a capillary breach. Its peak width corresponds to the instrument energy resolution at each Q. Because a higher energy neutron was used at a higher Q, the width of elastic line is broader for $Q = 5.18 \pm 0.05$ Å^{-1} as seen in the figure. The inelastic scattering profile is relatively featureless. Therefore, it is difficult to extract dynamical information without relying on extensive modeling in reciprocal space. Furthermore, observing both the coherent and incoherent scattering in $MgCl_2$ complicates the situation; the coherent scattering cross section of Mg and Cl are 3.631 barn and 11.526 barn, respectively, and the incoherent scattering cross section of Mg and Cl are 0.08 barn and 5.3 barn, respectively.[27] The coherent scattering contributes to both the self-part and the distinct-part, while the incoherent scattering contributes only to the self-part. Therefore, it is complicated to decompose the self-motion and correlated motion in reciprocal space.

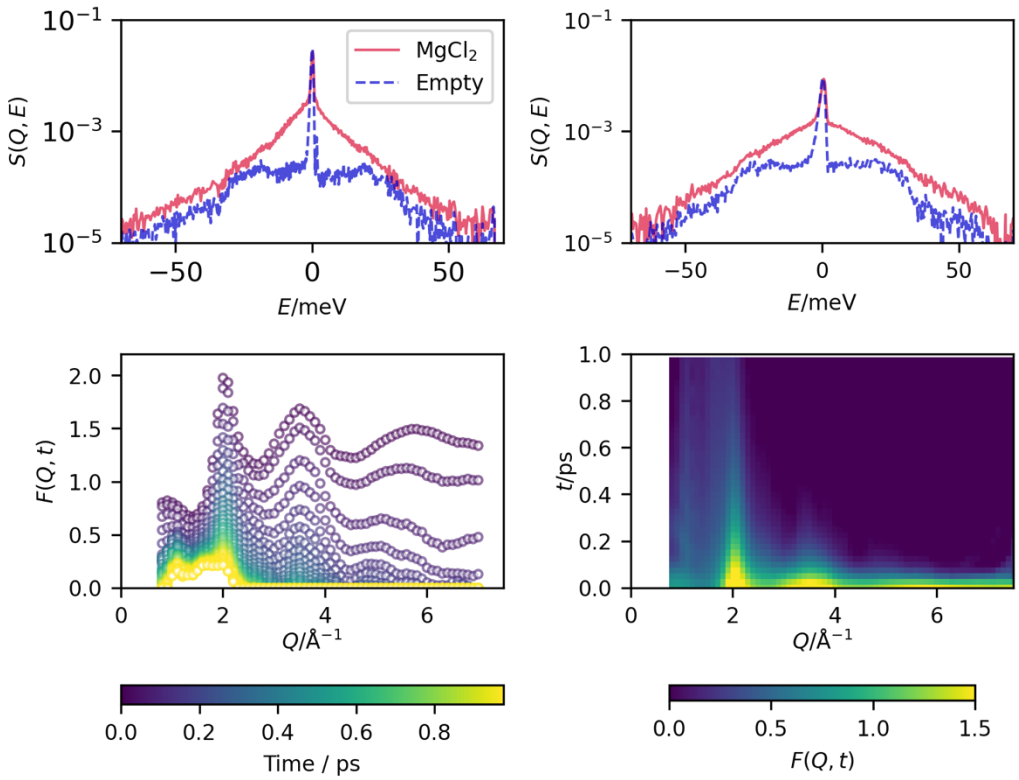

Figure 1. (Top panels) Dynamic structure function $S(Q,E)$ of (solid line) molten $MgCl_2$ and (dashed line) the empty sample container at (left) Q = 3.88 ± 0.05 Å^{-1} and (right) 5.18 ± 0.05 Å^{-1}. (Bottom panels) Intermediate scattering function of molten $MgCl_2$. The minimum Q in the spectra, Q_{min}, is 0.7 Å^{-1}. The left figure shows the one-dimensional slice at $0 \le t \le 1$ ps and the right figure shows their intensity map. Their color scales are shown on the bottom. In the one-dimensional slice, the interval between each time slice is 0.025 ps.

Following our previous INS and IXS experiments on other types of liquid,[14,16,17] we obtained the intermediate scattering function, $F(Q,t)$, by calculating the Fourier transformation of $S(Q,E)$ over E as shown in Figure 1 (bottom). At a short timescale ($t \le 0.075$ ps), $F(Q,t)$ at the highest Q shows a finite value. The finite values at a cut-off position result in a substantial termination error when the spectra are converted to the real space. However, at a longer time, the value of $F(Q,t)$ at the highest Q is close enough to zero, minimizing the effect of termination errors as

demonstrated previously[16]. At low-Q, we did not extrapolate the data to $Q = 0$, and this influences the longer length scale profiles in the VHF but has much less effect on the shape of peaks in our current discussion.

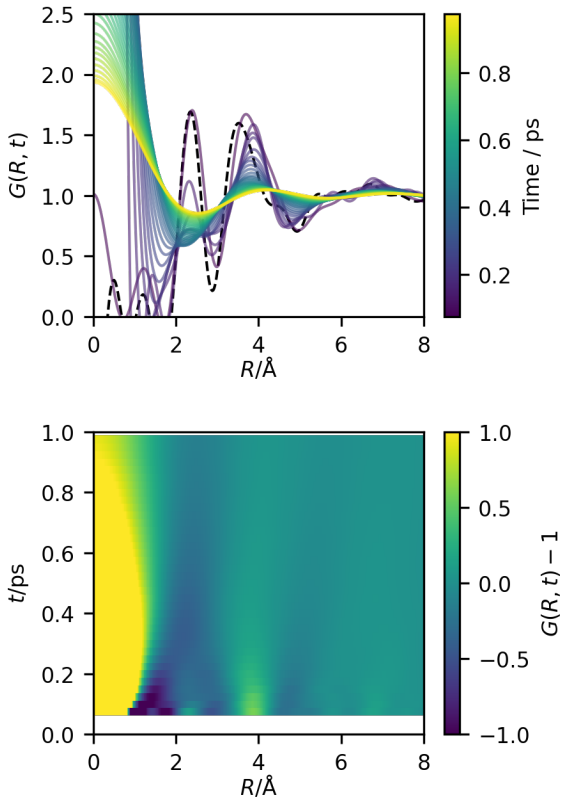

Figure 2. (Top) One-dimensional profiles of $G(R,t)$ of 0.075 < t/ps < 1.0 and (bottom) intensity map of $G(R,t) - 1$ magnesium chloride molten salt, calculated from the INS measurement. The dashed line in the top panel is a snap-shot PDF calculated from the total neutron scattering measurements[8].

Figure 2 shows the VHF obtained by calculating the Fourier transformation of $F(Q,t)$ over Q. To avoid the confusion due to the termination errors, $G(R, t < 0.075\ \text{ps})$ is excluded from the figure. In the upper panel, the snap-shot PDF of molten $MgCl_2$ calculated by the Fourier transform of the total neutron scattering data by Biggin et al.[8] at 725 ˚C with Q_{max} = 10 Å^{-1} is also shown as

a reference for $G(R, t = 0)$. The self-part of $G(R, t)$ is predominant at $R < 1.5$ Å, while the distinct part at a larger R shows the inter-ionic correlations. The self-part originates from both incoherent and coherent neutron scattering of molten $MgCl_2$, while the distinct part stems only from coherent neutron scattering. In this way, we can separate the information of self-motion and correlated motions in real space, although the self-part and the distinct part gradually start to overlap at a longer t. At $R = 2.37$ Å, a positive peak corresponding to the nearest neighbor correlation between the magnesium ion and the chloride ion is found. This correlation of opposite charge ions Mg^{2+}–Cl^- is quickly lost before 0.15 ps. At $R = 3.8$ Å, another positive peak is observed, which corresponds to the next nearest-neighbor correlation between same charge ions: Cl^-–Cl^- and Mg^{2+}–Mg^{2+}.[8] The decaying behavior of height and area of this second-neighbor peak is shown in Figure 3. It decays in sub-ps, which is comparable to the decay time observed in water at room temperature.[28] The decaying behavior can be characterized by a two-step decay; the first steep decay ($t < \sim 0.3$ ps) that may be characterized by a compressed exponential decay and a subsequent long-time decay that can be characterized by an exponential decaying function. A similar two-step decaying behavior has been observed for the nearest-neighbor correlation in water[28] and aqueous salt solutions[29] and was interpreted as the first decay representing ballistic-like motion, and the slower decay representing the correlation between ions. The latter is likely to be related to viscosity, following the observation by simulation that local configurational changes are directly related to macroscopic viscosity.[30] Interestingly, the macroscopic viscosity of molten $MgCl_2$ (1.54 mPa·s at 875 ˚C)[31] is comparable to that of water at room temperature (1.01 mPa·s at 20 ˚C)[32], suggesting a possible universal connection between local configurational changes and macroscopic viscosity of liquids despite the drastically different types of bonding.

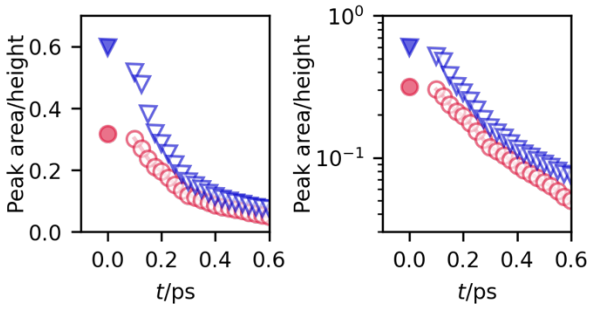

Figure 3. Decaying behavior of correlation peak at around R = 3.8 Å in (left) linear scale and (right) semi-log scale. Peak height and peak area are denoted by triangles and circles, respectively. The filled symbols are the values extracted by a snap-shot neutron PDF data[8]. Uncertainty due to the neutron counting statistics and the way of correcting energy resolution is smaller than the size of symbols.

One of the most striking features in $G_{\mathrm{d}}(R,t)$ is that the correlation between same charge ions decays much more slowly than the nearest-neighbor correlation between opposite charge ions. In general, the relaxation time in the VHF increases monotonically with distance because of the geometrical reason as shown for simple model liquids,[33] but the significant difference in the current study indicates that the correlated motion between same charge ions and that between opposite charge ions are quite different. This difference recalls a recent study showing that the configuration of molten $MgCl_2$ displays the formation of chloride ion-decorated Mg^{2+} chains in contrast to a prototypical salt in which structure is governed by simple charge alternation[34]. For further discussion, distinguishing the dynamics of Mg^{2+}–Mg^{2+} correlation from those of Cl^-–Cl^- correlation using element specific analyses would be very insightful, but the current data do not allow disentangling the Cl^-–Cl^- and Mg^{2+}–Mg^{2+} correlations because they appear at similar distances and their peak widths are intrinsically broad. In the conventional neutron PDF studies of molten salt, isotopic substitution was used to modify the scattering contrast, thereby enabling the

element-specific partial correlation functions in various kinds of molten salt systems.[8,35–38] A VHF study with a similar contrast variation technique via isotopic substitution will be crucial in disentangling multi-component dynamics by providing the partial dynamic structure factor and partial VHF. However, such a study is out of scope for this work aimed at establishing the applicability of the VHF approach to investigate local dynamics in molten salts.

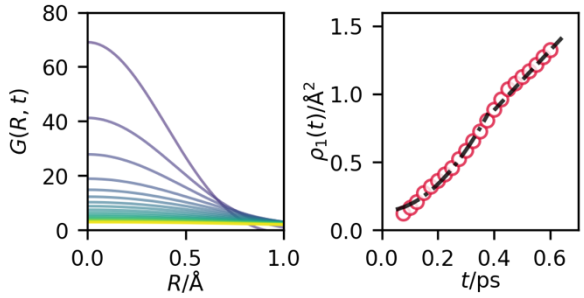

Figure 4. The Van Hove correlation function at around $R = 0$ (left). Start from $t = 0.075$ ps. $\Delta t = 0.025$ ps. Mean-square displacement function (right) derived from the Gaussian approximation of $G_s(R,t)$ of $MgCl_2$. The dashed line is a long-time fit, $2Dt$, with $D = 1.1$ Å^2/ps and the dotted line is a short time fit with ${v_0}^2t^2 + \rho_0$ with ${v_0}^2 = 2.23$ Å/ps and $\rho_0 = 0.14$ Å^2. Uncertainty estimated by the standard deviation of the fitting was smaller than the size of the symbols.

Now we shift our attention onto the self-part of the VHF, $G_s(R,t)$, which is observed at around $R = 0$ (Figure 4). The conversion into the real-space correlation function enables us to distinguish the self-part from the distinct-part at a short timescale until the particles move in a distance comparable to the nearest-neighbor distance, leading to the significant overlap between the signals from the self-part and the distinct part. As in the previous work on water[16], the self-part is well described by the assumption of the Gaussian approximation[39], which represents the self-part of the VHF by

$$G_s(R,t) = [2\pi\rho_1(t)]^{-3/2}\exp[-R^2/2\rho_1(t)],$$

where $\rho_1(t)$ is the mean-square displacement function[40]. $\rho_1(t)$ in Figure 4 (right) is similar to those obtained in liquid argon derived from neutron incoherent scattering[41], although our dataset is limited to $t < 0.7$ ps mainly because the contributions from the distinct part cannot be ignored at a large R at a large t and the Gaussian approximation cannot be applied unambiguously[16]. A long-time fit using $2Dt$ provides the diffusion coefficient $D = 1.1$ Å^2/ps at $t > 0.4$ ps. To our knowledge, there is currently no experimental data available on macroscopic diffusion coefficient of Mg^{2+} and Cl^- in pure $MgCl_2$, but the obtained value is consistent with those for Mg^{2+} and Cl^- in different melts[42–44]. We also attempted to model the self-part by using two Gaussian functions representing Cl^- diffusion and Mg^{2+} diffusion, but fitting by two Gaussian functions did not work well presumably because the contribution of Cl^- is much higher due to its higher coherent and incoherent scattering cross section and a double amount based on the stoichiometry of magnesium chloride.

In addition to providing fundamental insights into the dynamic structural behavior of molten salts, the current VHF approach could serve as an end-member benchmark for the existing density functional theory (DFT) and classical MD methods. Recent AIMD studies of molten $MgCl_2$ using several flavors of DFT showed that only PBE-D3 density functional[45,46] successfully reproduced the experimental Raman spectrum, while all of them reproduced a snap-shot structure, namely, the PDF determined by total neutron and X-ray scattering,[34] suggesting that different types of DFT should be employed with caution for predicting experimental observables. As recently demonstrated for water,[47] we will be able to develop more reliable simulation models in terms of atomic-scale dynamics by comparing experimental VHFs with VHFs calculated based on AIMD.

In summary, we have successfully visualized the real-space local correlations of ions in molten ionic media at high temperatures that is hard to recognize and study in reciprocal space. The results

clarified the apparent difference in the correlated motion of same vs. opposite charge ions, which is presumably due to the formation of chloride ion-decorated Mg^{2+} chains.[34] This has been achieved by measuring the INS of molten $MgCl_2$ in extreme environments at high temperatures and converting the INS spectra into the real-space temporal correlation function, VHF, via the Fourier transform over *E* and *Q*. Having established an approach for determining the self and correlated local motions via the VHFs, further advances in fundamental understanding of molten salt dynamics can be expected. Future studies employing isotope substitution will help disentangle the real-space local dynamics of different ion-pair correlations. Critical knowledge obtained through the VHFs of molten salts is also expected to serve as a benchmark for testing and development of accurate atomistic AIMD models and machine-learning potentials[48,49] for large-scale MD simulations, significantly enhancing our ability to predict the local dynamics of condensed matter in extreme environments, with pertinence to emergent carbon-free solar energy storage and nuclear reactor technologies.

Methods

Time-of-flight INS measurements were carried out using wide-angular range chopper spectrometer (ARCS)[25] at the Spallation Neutron Source (SNS), Oak Ridge National Laboratory. Three incident energies, 20, 40, and 80 meV, were used to balance the wide *Q*-*E* range and the *Q*- and *E*- resolution to achieve the conversion into the Van Hove correlation function. The measurements were performed using the Fermi chopper slit package (ARCS-100-1.5) spinning at 240 Hz (20 meV), 360 Hz (40 meV), and 480 Hz (80 meV). The instrumental energy resolution was 3-5 % of the incident energy[25]. Anhydrous $MgCl_2$ (99.9%) was purchased from Sigma Aldrich and further purified by distillation. To minimize the effect of self-shielding and multiple scattering, the salt was put into five thin-walled quartz cylinder cells (2.0 mm O.D. and 0.010 mm wall

thickness, Charles Supper) in a glove box. The capillaries were flame sealed near the top under vacuum. The quartz capillaries were assembled in a planar geometry and were covered by a Vanadium foil to avoid the damage to a furnace in the event of a capillary failure. The use of the thin-walled cylinder with a small radius decreased the signal intensity of sample scattering relative to the background scattering from the furnace (mostly vanadium), but it drastically reduces the self-shielding and multiple scattering due to the samples and quartz capillaries. Note that the scattering from vanadium is incoherent, so insufficient subtraction of the scattering from vanadium mostly contributes to the self-part of the VHF after conversion. MICAS furnace[50] was used to control the sample temperature at 875 ˚C. The scattering data were collected for about 1.5 h for each incident energy with 1.4 MW operation. The background including the empty container was measured using the three incident neutron energies. Data up to Q = 7.0 Å^{-1} were used and were reduced using the Mantid suites.[51] The data were symmetrized by using a detailed balance factor before being merged with data taken with other incident neutron energies. Following our previous IXS studies,[14,28] the data were also normalized to the absolute scale by $S(Q,E) = \frac{S_n(Q)}{\int S_{\mathrm{raw}}(Q,E)\mathrm{d}E} S_{\mathrm{raw}}(Q,E)$, where $S_{\mathrm{raw}}(Q,E)$ were the symmetrized neutron scattering spectra and $S_n(Q)$ is a total neutron scattering profile of molten $MgCl_2$ and incoherent scattering contribution. Considering the mean free path of neutrons (20, 40, and 80 meV) is orders of magnitude larger than the capillary radius, we analyzed the scattering spectra without any correction for multiple scattering, but an absorption correction was done considering the energy difference before and after the scattering because of a large absorption cross-section of Cl. The effect of instrument energy resolution was removed in the time domain by dividing the intermediate scattering function by the Fourier transform of the instrument energy resolution function over energy[29]. The energy

resolution at each Q was represented by the value at the elastic line, where there is no energy transfer.

AUTHOR INFORMATION

Corresponding Authors

*Email: shinoharay@ornl.gov (Y.S.)

*Email: ivanova@ornl.gov (A.S.I.)

ORCID

Yuya Shinohara: 0000-0001-8284-751X

Alexander S. Ivanov: 0000-0002-8193-6673

Dmitry Maltsev: 0000-0001-5678-1465

Garrett E. Granroth: 0000-0002-7583-8778

Douglas L. Abernathy: 0000-0002-3533-003X

Sheng Dai: 0000-0002-8046-3931

Takeshi Egami: 0000-0002-1126-0276

Notes

The authors declare no competing financial interests.

ACKNOWLEDGMENT

Work by Y. S. and T. E. was supported by U.S. Department of Energy (DOE), Office of Science, Office of Basic Energy Science, Division of Materials Sciences and Engineering. Work by A. S.

I, D. M. and S. D. was supported as part of the Molten Salts in Extreme Environments (MSEE) Energy Frontier Research Center. A portion of this research used resources at Spallation Neutron Source, a DOE Office of Science User Facility operated by Oak Ridge National Laboratory.

REFERENCES

(1) Williams, D. F.; Britt, P. F. *Technology and Applied R&D Needs for Molten Salt Chemistry: Innovative Approaches to Accelerate Molten Salt Reactor Development and Deployment*. Report for the US Department of Energy, Office of Nuclear Energy Workshop, Molten Salt Chemistry Workshop at Oak Ridge National Laboratory, 2017.
(2) Revere, M.; Tosi, M. P. Structure and Dynamics of Molten Salts. *Rep. Prog. Phys.* **1986**, *49*, 1001–1081.
(3) Le Brun, C. Molten Salts and Nuclear Energy Production. *J. Nucl. Mater.* **2007**, *360*, 1–5.
(4) MacPherson, H. G. The Molten Salt Reactor Adventure. *Nucl. Sci. Eng.* **1985**, *90*, 374–380.
(5) LeBlanc, D. Molten Salt Reactors: A New Beginning for an Old Idea. *Nucl. Eng. Des.* **2010**, *240*, 1644–1656.
(6) Xu, X.; Wang, X.; Li, P.; Li, Y.; Hao, Q.; Xiao, B.; Elsentriecy, H.; Gervasio, D. Experimental Test of Properties of KCl–$MgCl_2$ Eutectic Molten Salt for Heat Transfer and Thermal Storage Fluid in Concentrated Solar Power Systems. *J. Sol. Energy Eng.* **2018**, *140*, 051011.
(7) Zhao, Y.; Vidal, J. Potential Scalability of a Cost-Effective Purification Method for $MgCl_2$-Containing Salts for next-Generation Concentrating Solar Power Technologies. *Sol. Energy Mater. Sol. Cells* **2020**, *215*, 110663.
(8) Biggin, S.; Gay, M.; Enderby, J. E. The Structures of Molten Magnesium and Manganese (II) Chlorides. *J. Phys. C Solid State Phys.* **1984**, *17*, 977–986.
(9) Wilson, M.; Madden, P. A. Short- and Intermediate-Range Order in MCl_2 Melts: The Importance of Anionic Polarization. *J. Phys. Condens. Matter* **1993**, *5*, 6833–6844.
(10) McGreevy, R. L.; Mitchell, E. W. J. Collective Modes in Molten Alkaline Earth Chlorides: III. Inelastic Neutron Scattering from Molten $MgCl_2$ and $CaCl_2$. *J. Phys. C Solid State Phys.* **1985**, *18*, 1163–1178.
(11) Roy, S.; Wu, F.; Wang, H.; Ivanov, A. S.; Sharma, S.; Halstenberg, P.; Gill, S. K.; Milinda Abeykoon, A. M.; Kwon, G.; Topsakal, M.; Layne, B.; Sasaki, K.; Zhang, Y.; Mahurin, S. M.; Dai, S.; Margulis, C. J.; Maginn, E. J.; Bryantsev, V. S. Structure and Dynamics of the Molten Alkali-Chloride Salts from an X-Ray, Simulation, and Rate Theory Perspective. *Phys. Chem. Chem. Phys.* **2020**, *22*, 22900–22917.
(12) Roy, S.; Brehm, M.; Sharma, S.; Wu, F.; Maltsev, D. S.; Halstenberg, P.; Gallington, L. C.; Mahurin, S. M.; Dai, S.; Ivanov, A. S.; Margulis, C. J.; Bryantsev, V. S. Unraveling Local Structure of Molten Salts via X-Ray Scattering, Raman Spectroscopy, and *Ab Initio* Molecular Dynamics. *J. Phys. Chem. B* **2021**, *125*, 5971–5982.
(13) Luo, P.; Zhai, Y.; Leao, J. B.; Kofu, M.; Nakajima, K.; Faraone, A.; Z, Y. Neutron Spin–Echo Studies of the Structural Relaxation of Network Liquid $ZnCl_2$ at the Structure Factor Primary Peak and Prepeak. *J. Phys. Chem. Lett.* **2021**, *12*, 392–398.

(14) Iwashita, T.; Wu, B.; Chen, W.-R.; Tsutsui, S.; Baron, A. Q. R.; Egami, T. Seeing Real-Space Dynamics of Liquid Water through Inelastic X-Ray Scattering. *Sci. Adv.* **2017**, *3*, e1603079.
(15) Shinohara, Y.; Matsumoto, R.; Thompson, M. W.; Ryu, C. W.; Dmowski, W.; Iwashita, T.; Ishikawa, D.; Baron, A. Q. R.; Cummings, P. T.; Egami, T. Identifying Water–Anion Correlated Motion in Aqueous Solutions through Van Hove Functions. *J. Phys. Chem. Lett.* **2019**, *10*, 7119–7125.
(16) Shinohara, Y.; Dmowski, W.; Iwashita, T.; Ishikawa, D.; Baron, A. Q. R.; Egami, T. Local Self-Motion of Water through the Van Hove Function. *Phys. Rev. E* **2020**, *102*, 032604.
(17) Ashcraft, R.; Wang, Z.; Abernathy, D. L.; Quirinale, D. G.; Egami, T.; Kelton, K. F. Experimental Determination of the Temperature-Dependent Van Hove Function in a $Zr_{80}Pt_{20}$ Liquid. *J. Chem. Phys.* **2020**, *152*, 074506.
(18) Kawakita, Y.; Kikuchi, T.; Inamura, Y.; Tahara, S.; Maruyama, K.; Hanashima, T.; Nakamura, M.; Kiyanagi, R.; Yamauchi, Y.; Chiba, K.; Ohira-Kawamura, S.; Sakaguchi, Y.; Shimakura, H.; Takahashi, R.; Nakajima, K. Anomaly of Structural Relaxation in Complex Liquid Metal of Bismuth - Dynamic Correlation Function of Coherent Quasi-Elastic Neutron Scattering. *Phys. B Condens. Matter* **2018**, *551*, 291–296.
(19) Van Hove, L. Correlations in Space and Time and Born Approximation Scattering in Systems of Interacting Particles. *Phys. Rev.* **1954**, *95*, 249–262.
(20) Dahlborg, U.; Gudowski, W.; Davidovic, M. Van Hove Correlation Functions from Coherent Neutron Inelastic Scattering. *J. Phys. Condens. Matter* **1989**, *1*, 6173–6179.
(21) Brockhouse, B. N.; Pope, N. K. Time-Dependent Pair Correlations in Liquid Lead. *Phys. Rev. Lett.* **1959**, *3*, 259–262.
(22) Stone, M. B.; Niedziela, J. L.; Abernathy, D. L.; DeBeer-Schmitt, L.; Ehlers, G.; Garlea, O.; Granroth, G. E.; Graves-Brook, M.; Kolesnikov, A. I.; Podlesnyak, A.; Winn, B. A Comparison of Four Direct Geometry Time-of-Flight Spectrometers at the Spallation Neutron Source. *Rev. Sci. Instrum.* **2014**, *85*, 045113.
(23) Baron, A. Q. R. High-Resolution Inelastic X-Ray Scattering I: Context, Spectrometers, Samples, and Superconductors. In *Synchrotron Light Sources and Free-Electron Lasers*; Jaeschke, E. J., Khan, S., Schneider, J. R., Hastings, J. B., Eds.; Springer International Publishing: Cham, **2016**, 1643–1719.
(24) Baron, A. Q. R. High-Resolution Inelastic X-Ray Scattering II: Scattering Theory, Harmonic Phonons, and Calculations. In *Synchrotron Light Sources and Free-Electron Lasers*; Jaeschke, E., Khan, S., Schneider, J. R., Hastings, J. B., Eds.; Springer International Publishing: Cham, **2016**, 1721–1757.
(25) Abernathy, D. L.; Stone, M. B.; Loguillo, M. J.; Lucas, M. S.; Delaire, O.; Tang, X.; Lin, J. Y. Y.; Fultz, B. Design and Operation of the Wide Angular-Range Chopper Spectrometer ARCS at the Spallation Neutron Source. *Rev. Sci. Instrum.* **2012**, *83*, 015114.
(26) Mason, T. E.; Abernathy, D.; Anderson, I.; Ankner, J.; Egami, T.; Ehlers, G.; Ekkebus, A.; Granroth, G.; Hagen, M.; Herwig, K.; Hodges, J.; Hoffmann, C.; Horak, C.; Horton, L.; Klose, F.; Larese, J.; Mesecar, A.; Myles, D.; Neuefeind, J.; Ohl, M.; Tulk, C.; Wang, X.-L.; Zhao, J. The Spallation Neutron Source in Oak Ridge: A Powerful Tool for Materials Research. *Phys. B Condens. Matter* **2006**, *385–386*, 955–960.
(27) Sears, V. F. Neutron Scattering Lengths and Cross Sections. *Neutron News* **1992**, *3*, 26–37.
(28) Shinohara, Y.; Dmowski, W.; Iwashita, T.; Wu, B.; Ishikawa, D.; Baron, A. Q. R.; Egami, T. Viscosity and Real-Space Molecular Motion of Water: Observation with Inelastic X-Ray Scattering. *Phys. Rev. E* **2018**, *98*, 022604.

(29) Shinohara, Y.; Dmowski, W.; Iwashita, T.; Ishikawa, D.; Baron, A. Q. R.; Egami, T. Local Correlated Motions in Aqueous Solution of Sodium Chloride. *Phys. Rev. Mater.* **2019**, *3*, 065604.
(30) Iwashita, T.; Nicholson, D. M.; Egami, T. Elementary Excitations and Crossover Phenomenon in Liquids. *Phys. Rev. Lett.* **2013**, *110*, 205504.
(31) Janz, G. J.; Tomkins, R. P. T.; Allen, C. B.; Downey, J. R.; Garner, G. L.; Krebs, U.; Singer, S. K. Molten Salts: Volume 4, Part 2, Chlorides and Mixtures—Electrical Conductance, Density, Viscosity, and Surface Tension Data. *J. Phys. Chem. Ref. Data* **1975**, *4*, 871–1178.
(32) Kestin, J.; Sokolov, M.; Wakeham, W. A. Viscosity of Liquid Water in the Range −8 °C to 150 °C. *J. Phys. Chem. Ref. Data* **1978**, *7*, 941–948.
(33) Wu, B.; Iwashita, T.; Egami, T. Atomic Dynamics in Simple Liquid: De Gennes Narrowing Revisited. *Phys. Rev. Lett.* **2018**, *120*, 135502.
(34) Wu, F.; Roy, S.; Ivanov, A. S.; Gill, S. K.; Topsakal, M.; Dooryhee, E.; Abeykoon, M.; Kwon, G.; Gallington, L. C.; Halstenberg, P.; Layne, B.; Ishii, Y.; Mahurin, S. M.; Dai, S.; Bryantsev, V. S.; Margulis, C. J. Elucidating Ionic Correlations Beyond Simple Charge Alternation in Molten $MgCl_2$–KCl Mixtures. *J. Phys. Chem. Lett.* **2019**, *10*, 7603–7610.
(35) Edwards, F. G.; Enderby, J. E.; Howe, R. A.; Page, D. I. The Structure of Molten Sodium Chloride. *J. Phys. C Solid State Phys.* **1975**, *8*, 3483–3490.
(36) Biggin, S.; Enderby, J. E. Comments on the Structure of Molten Salts. *J. Phys. C Solid State Phys.* **1982**, *15*, L305–L309.
(37) Skinner, L. B.; Benmore, C. J.; Weber, J. K. R.; Tumber, S.; Lazareva, L.; Neuefeind, J.; Santodonato, L.; Du, J.; Parise, J. B. Structure of Molten $CaSiO_3$: Neutron Diffraction Isotope Substitution with Aerodynamic Levitation and Molecular Dynamics Study. *J. Phys. Chem. B* **2012**, *116*, 13439–13447.
(38) Li, Q.-J.; Sprouster, D.; Zheng, G.; Neuefeind, J. C.; Braatz, A. D.; Mcfarlane, J.; Olds, D.; Lam, S.; Li, J.; Khaykovich, B. Complex Structure of Molten NaCl–$CrCl_3$ Salt: Cr–Cl Octahedral Network and Intermediate-Range Order. *ACS Appl. Energy Mater.* **2021**, *4*, 3044–3056.
(39) Vineyard, G. H. Scattering of Slow Neutrons by a Liquid. *Phys. Rev.* **1958**, *110*, 999–1010.
(40) Boon, J. P.; Yip, S. *Molecular Hydrodynamics*; McGraw-Hill, New York, 1980.
(41) Sköld, K.; Rowe, J. M.; Ostrowski, G.; Randolph, P. D. Coherent- and Incoherent-Scattering Laws of Liquid Argon. *Phys. Rev. A* **1972**, *6*, 1107–1131.
(42) Rao, G. M. Electrochemical Studies of Magnesium Ions in Magnesium Chloride Containing Chloride Melt at 710±10˚C. *J. Electroanal. Chem.* **1988**, *249*, 191–203.
(43) Tang, H.; Yan, Y-D.; Zhang, M-L.; Xue, Y.; Zhang, Z.-J.; Du, W.-C.; He, H.; Electrochemistry of $MgCl_2$ in LiCl-KCl Eutectic Melts. *Acta Phys.-Chim. Sin.* **2013**, *29*, 1698–1704.
(44) Janz, G. J.; Bansal, N. P. Molten Salts Data: Diffusion Coefficients in Single and Multi-Component Salt Systems. *J. Phys. Chem. Ref. Data* **1982**, *11*, 505–693.
(45) Perdew, J. P.; Burke, K.; Ernzerhof, M. Generalized Gradient Approximation Made Simple. *Phys. Rev. Lett.* **1996**, *77*, 3865–3868.
(46) Grimme, S.; Antony, J.; Ehrlich, S.; Krieg, H. A Consistent and Accurate *Ab Initio* Parametrization of Density Functional Dispersion Correction (DFT-D) for the 94 Elements H-Pu. *J. Chem. Phys.* **2010**, *132*, 154104.
(47) Matsumoto, R. A.; Thompson, M. W.; Vuong, V. Q.; Zhang, W.; Shinohara, Y.; van Duin, A. C. T.; Kent, P. R. C.; Irle, S.; Egami, T.; Cummings, P. T. Investigating the Accuracy of

Water Models through the Van Hove Correlation Function. *J. Chem. Theory Comput.* **2021**, *17*, 5992–6005.
(48) Sivaraman, G.; Guo, J.; Ward, L.; Hoyt, N.; Williamson, M.; Foster, I.; Benmore, C.; Jackson, N. Automated Development of Molten Salt Machine Learning Potentials: Application to LiCl. *J. Phys. Chem. Lett.* **2021**, *12*, 4278–4285.
(49) Li, Q.-J.; Kücükbenli, E.; Lam, S.; Khaykovich, B.; Kaxiras, E.; Li, J. Development of Robust Neural-Network Interatomic Potential for Molten Salt. *Cell Rep. Phys. Sci.* **2021**, *2*, 100359.
(50) Niedziela, J. L.; Mills, R.; Loguillo, M. J.; Skorpenske, H. D.; Armitage, D.; Smith, H. L.; Lin, J. Y. Y.; Lucas, M. S.; Stone, M. B.; Abernathy, D. L. Design and Operating Characteristic of a Vacuum Furnace for Time-of-Flight Inelastic Neutron Scattering Measurements. *Rev. Sci. Instrum.* **2017**, *88*, 105116.
(51) Arnold, O.; Bilheux, J. C.; Borreguero, J. M.; Buts, A.; Campbell, S. I.; Chapon, L.; Doucet, M.; Draper, N.; Ferraz Leal, R.; Gigg, M. A.; Lynch, V. E.; Markvardsen, A.; Mikkelson, D. J.; Mikkelson, R. L.; Miller, R.; Palmen, K.; Parker, P.; Passos, G.; Perring, T. G.; Peterson, P. F.; Ren, S.; Reuter, M. A.; Savici, A. T.; Taylor, J. W.; Taylor, R. J.; Tolchenov, R.; Zhou, W.; Zikovsky, J. Mantid—Data Analysis and Visualization Package for Neutron Scattering and μSR Experiments. *Nucl. Instrum. Methods Phys. Res. A* **2014**, *764*, 156–166.